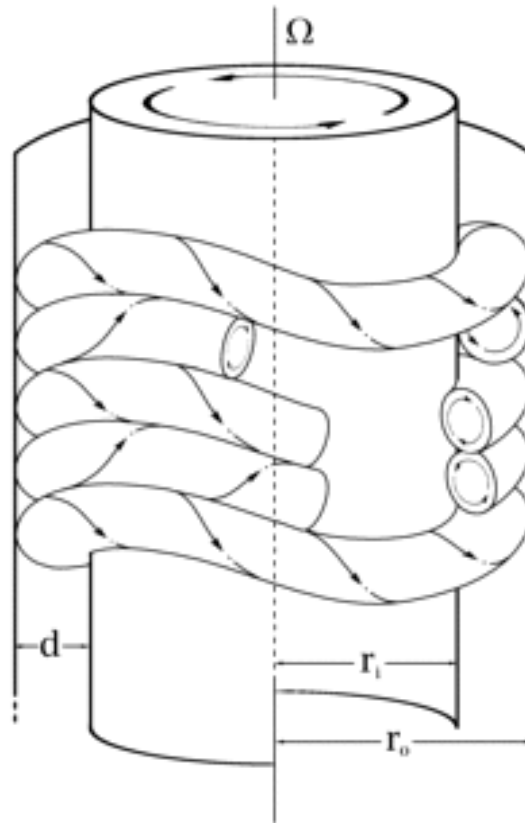# Masterthesis

Studiengang Maschinenbau
Fachrichtung Produktionstechnik und -management
HAW Hamburg

Untersuchung der linearen Stabilität der Taylor-Couette-Strömung mittels Polynomentwicklung höherer Ordnung

Erstellt von: *Patrick Diffo*

Betreut von: *Prof. Baumann*

Hamburg, 28.02.2011

Contents

List of Figures

List of Tables

1   Introduction and project definition

High Intensity Discharge (HID) lamps are light generating devices made of a ceramics or quartz arc tube also called burner which confines a gas mixture, usually mercury with some additives, and two electrodes. The imposition of current between these electrodes leads to the ionization of the gas, bringing it to temperatures between 5000 and 6000 K in a light-emitting region named the arc (see Figure 1 left). HID lamps find common applications in expansive outdoor spaces like streets, roadways, parking lots, stadiums, etc. The indoor applications, such as shop lighting, are on their side optimally operated at an alternate current frequency of around 300 kHz which can lead to an unstable plasma arc (lamp flicker in Figure 1 right) and even to an early lamp failure (paper Baumann). Acoustic resonance has been presumed for some years now to be the effect behind this arc instability [15]. For an accurate description of the effect's onset we refer to [14] and references therein. Since a new approach is undertaken, where an overlapping of the acoustic resonance with the temperature driven gas hydrodynamic instability is presumed.

In order to understand the phenomenon of hydrodynamic instability itself a more general problem of this kind has been chosen and an eigenvalue-problem has been set to be resolved in this work. It is the "Taylor-Couette" instability problem.
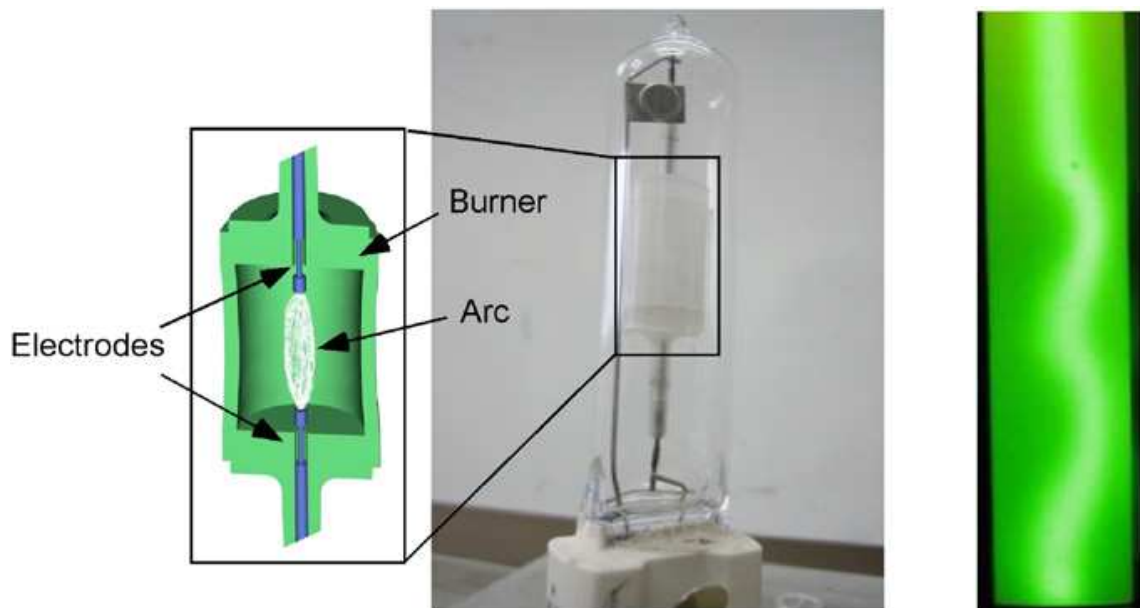
Figure 1: Structure of a HID lamp (left) and arc disturbed by acoustic resonance (right) [15]

Goal of the project is to analyse the stability of a Taylor-Couette-flow between differentially rotating concentric cylinders (inner cylinder rotating and outer cylinder fixed). Herefor a stability differential equations system is intended to be solved through development of a velocity field into first-kind Chebyshev polynomials at any order. This eigenvalue problem need be solved repetitively, each time for a different angular velocity (and thus different Reynolds number) over a broad wavenumber range.

The expected diagrams are:

- real part of maximal eigenvalue over wavenumber for each Reynolds number and

- maximum of the real part of maximal eigenvalue over Reynolds number

- influence of the choice of collocation points on the solution

Those should be compared with literature together with the resulting critical wavenumber, Reynolds number, at which the maximal eigenvalue turns positive (the fluid flow becomes unstable).

2   Hydrodynamic Instability

2.1   The Taylor-Couette-flow

The Taylor-Couette-flow is the name of the flow that occurs in the annulus between differentially rotating concentric cylinders, most often with the inner cylinder rotating and the outer cylinder fixed. The carried researches on this type of annular gap flow can be traced back 300 years ago where Isaac Newton started some studies on the topic. Building on the works of excellent theoreticians, like Max Margules or George Gabriel Stockes, Maurice Couette, a stellar Instrument builder, published 1888 the first experimental results of his viscosimeter. These results were then theoretically confirmed through the results of the linear stability theory of Geoffrey Ingram Taylor in 1923. Indeed the resulting stability diagram matched the experimental results in an unprecedental manner, which makes the Stability theory of Taylor one of the most influencial discoveries of the 20th century. His investigation was a key development in the modern study of fluid mechanics for three reasons (Donnelly 1991):

- It was taken by many as convincing proof of the no-slip boundary condition wherein the velocity of a particle in contact with a wall moves at the same velocity as the wall. Although this concept has become a fundamental tenet for the study of fluid flow, it was questioned until Taylor used it with such success in his analysis of the stability of Taylor-Couette flow.
- It offered convincing proof that the Navier-Stokes equations indeed accurately describe the flow of a Newtonian fluid, not just at the base flow level, but at a level that permitted the analysis of secondary flows and instabilities.
- It was the first successful application of linear stability analysis that accurately predicted experimental results, namely the transition from stable flow to vortical Taylor-Couette flow.

For scientists studying instabilities and transition phenomena this small closed system is appealing for experiments. Besides the Reynolds can be accurately controlled by cylindrical rotation rate and the use of glass tubes for the outer cylinder gives the flow visualization techniques access to the occurring flow pattern.

Fundamentals:

The shear flow arising from the mentioned rotation between the cylinders goes from a stable basic state to an unstable state at a critical ratio of cylinders' angular velocities. In its simplest form we let the inner cylinder rotate, while the outer cylinder is at rest and obtain the basic state flow, named Couette flow. Crosses the angular velocity of the in-

ner cylinder a "critical" number, instability occurs resulting in a pair of counter rotating, axisymmetric, toroidal vortices, which fill the annulus. This state is superimposed on the Couette flow.

Each pair of vortices has a wavelength of approximately $2d$, where $d = r_o - r_i$ is the gap between the cylinders.

Within a vortice a redistribution of angular momentum occurs through outward pushing of near inner wall high speed fluid, which carry the low speed outer wall fluid inwards.

The solution of the NSE for the stable state (Couette flow) gives us the radial velocity distribution over the annulus and states furthermore, that this stable state prevails thanks to the balance between the centrifugal force and the radial pressure within the fluid.

However, if a fluid particle is perturbed, that is, if it moves slightly outward from its initial status, it comes into a region of less pressure gradient arising, restoring force compared to the outward inertia of the particle. As a result the outward perturbed particle will continue outward. Likewise an inner perturbed fluid particle will continue inward. Thus, with the mass conservation insuring a return flow, a vortex in form of a toroid arises (see Figure 2). This instability is suppressed at low angular velocity by the viscosity through damping.

Would we rotate the outer cylinder and hold the inner one fixed, the flow would remain stable because the instability occurs only, when the pressure gradient force decreases with increasing radius.

Therefore the origin of the vortical flow is the centrifugal instability.
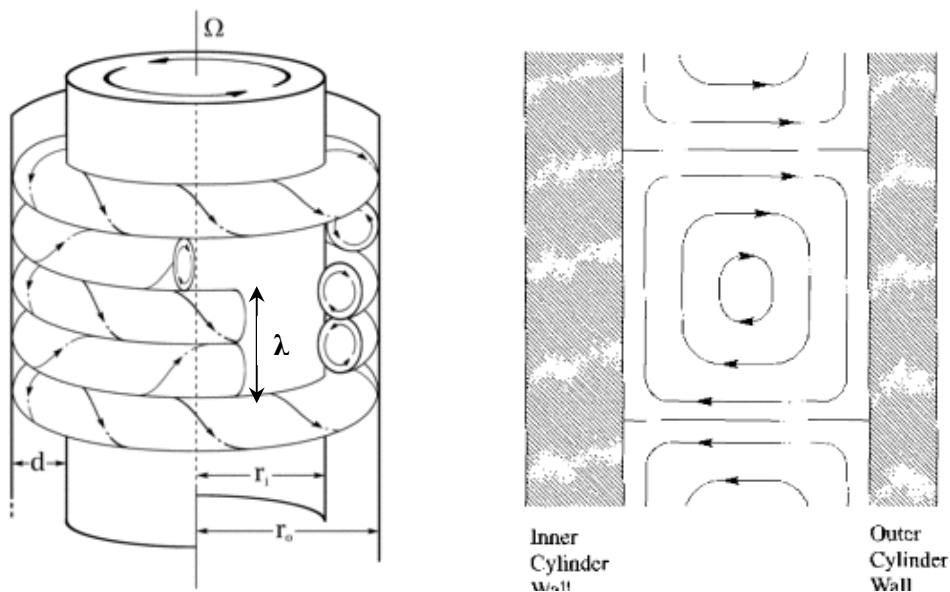
Figure 2: Axisymmetric Taylor vortices with inner cylinder rotating only [20]

Being already above the critical number, if we still increase the angular velocity of the inner cylinder, we than reach a secondary instability state, where the axisymmetric vortex flow (primary instability) become unstable. The new flow is called wavy vortex flow, which is characterized by azimuthal waviness of the vortices as shown schematically in Figure 3. The waves travel around the annulus at a speed that is 30-50% of the surface speed of the inner cylinder (King et al. 1984) and depend strongly on a dimensionless, radius ratio and angular velocity related number called "Taylor number".

a)   b)
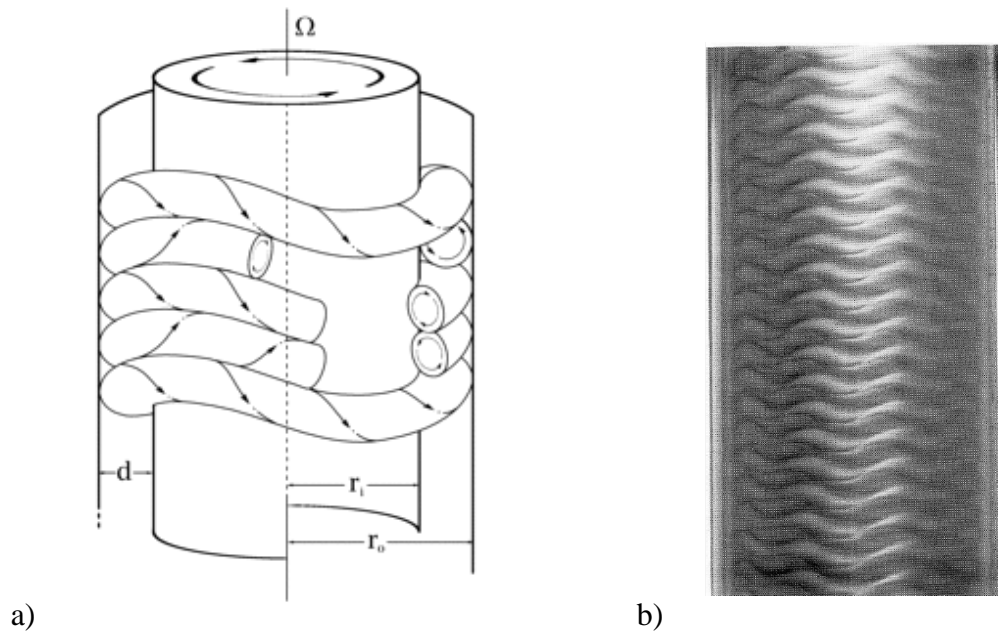
Figure 3: Counter-rotating wavy vortices, a)[20]   b)[8]

This state is followed by even higher order instabilities, as the modulated wavy vortex flow (see Figure 4), twisted vortex flow (see Figure 5) or spiral turbulence (see Figure 6).
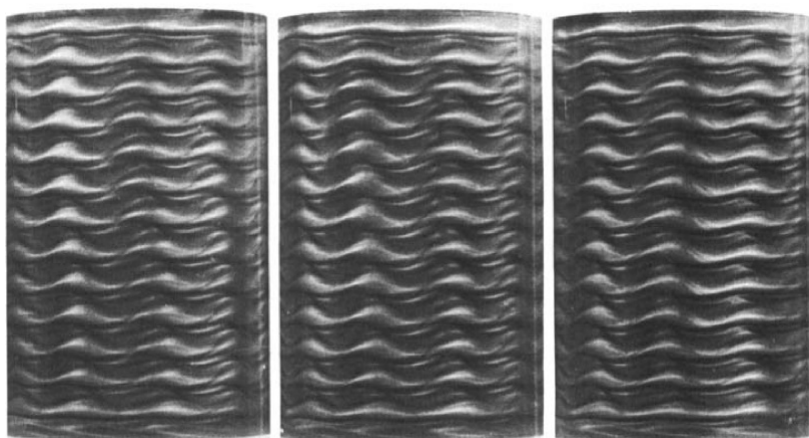
Figure 4: Modulated wavy vortex flow for $R_i = 350$, $R_o = -100$ [8]
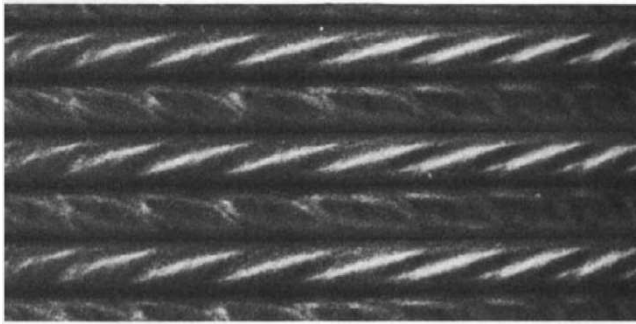
Figure 5: Twisted vortex flow [8]

a)   b)
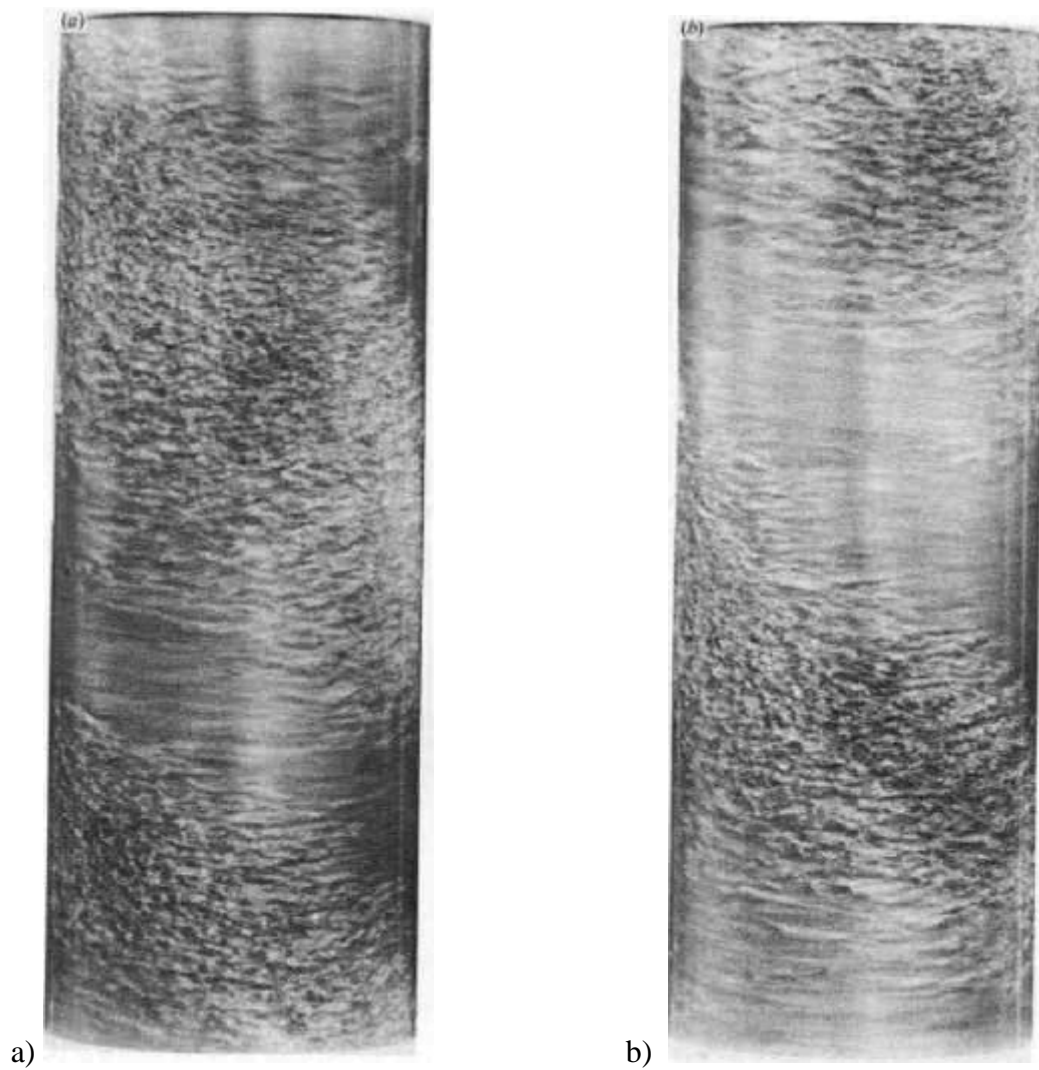
Figure 6: Spiral turbulence [8]

In Taylor-Couette geometries there are further instability modes. In the literature we find up to 74 different states (Coles 1965) depending on magnitude and orientation (counter or same rotating) of the cylinder. A few of these states are shown in Figure 7 together with the stable regime (Couette flow)
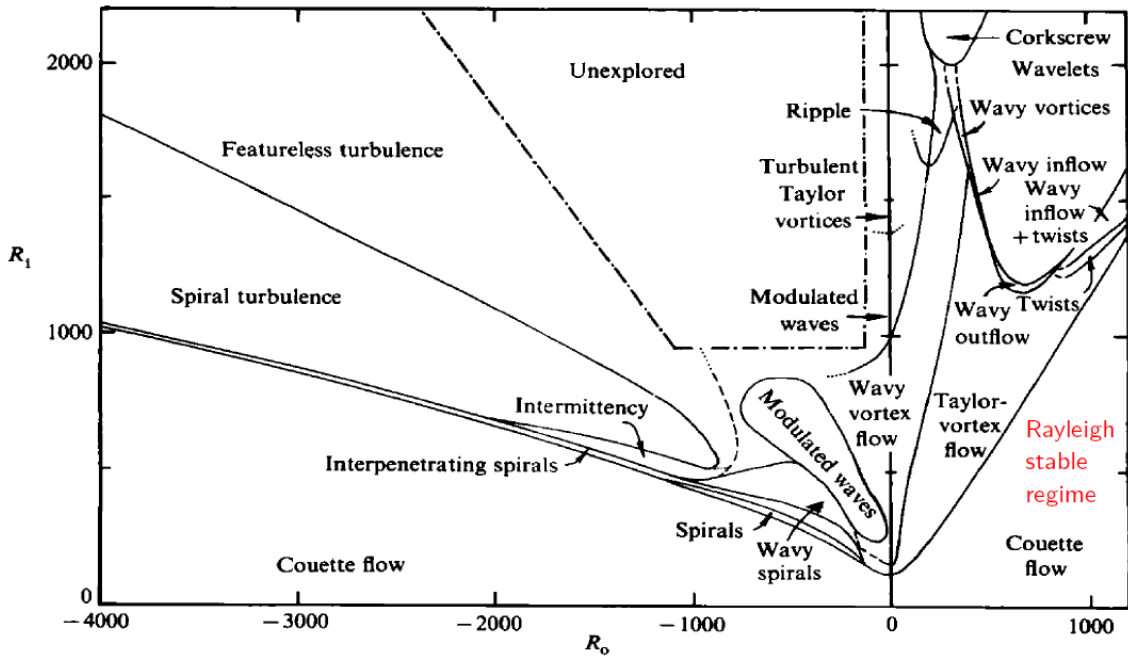
Figure 7: Flow regimes in a circular Couette system with independently rotating cylinders (Anderek et al. 1986)

3 Hydrodynamic Instability theory

3.1 Linear stability

Stability means physically the behaviour of a dynamical system toward a light perturbation from its equilibrium. It is clearly represented by the example of the behaviour of a sphere subjected to gravity and lying on differently formed surfaces (see Figure 8). On concave surfaces the sphere remains stable around its equilibrium. That is, through damping effects it returns autonomously to its point of equilibrium after having been displaced. On a horizontal surface we have an "indifferent" case, since the sphere doesn't oppose any reaction to the displacement. In the case of convex surfaces the sphere leaves its point of equilibrium by the slightest perturbation. The last case depicts the case of local stability, where the behaviour of the sphere depends on the magnitude of the perturbation.
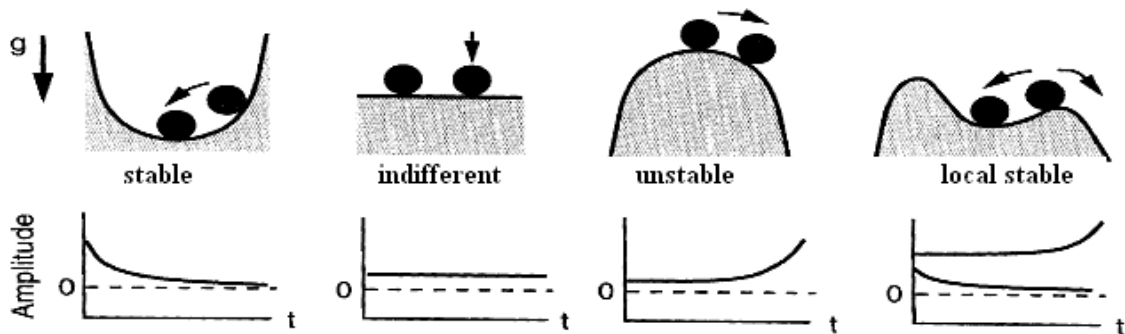
Figure 8: Definition of stability in the point mechanics [10]

For continua (fluids) the stability theory analyses (describes/predicts) the growth (or decay) of undulating perturbations *lower amplitudes* from a stationary (basic) state of the fluid. This definition means mathematically, that to the unknowns of the differential equation describing the dynamics of the physical phenomenon a small perturbation is added. By adding to an arbitrary basic state fluid velocity U and pressure P the perturbation *u* and *p*, respectively in the dimensionless, incompressible Navier-Stokes equation, we obtain for the perturbation the nonlinear differential equation system:

$$\frac{\partial u}{\partial t} + U.\nabla u + u.\nabla U + u.\nabla u = -\nabla p + \frac{1}{Re}\nabla^2 u \, ,$$

$$\nabla.u = 0.$$

With the boundary condition u = 0 or u = periodic.

In order to mathematically describe the term "stable" 3 approaches exist:

- *Lyapunov stability*, which requires that the norm of a perturbation around a basic state remains at all time less than a limit. The norm need not tend to 0 with growing time, but the solution never departs from the basic state in order to be named "stable".

- *Asymptotic stability*, which requires with the Lyapunov condition, that the norm of the perturbation should tend to 0 with growing time.

- *Exponential stability*, which exists when the norm of the perturbation follows the graph of an exponential function with growing time. The constant in the exponent defines the stability.

We focus our interest on the Lyapunov stability with the application of small perturbations. Thus, the quadratic, *non linear term* (u.Nab(u)) within the equation can be *neglected* and we obtain the *linear stability* problem:

$$\frac{\partial u}{\partial t} + U.\nabla u + u.\nabla U = -\nabla p + \frac{1}{Re}\nabla^2 u,$$

$$\nabla.u = 0.$$

With the boundary condition u=0 or u =periodic.

Depending on the problem, we can make an assumption regarding a possible solution for the equations. In most cases the *normal mode ansatz* is used. It is a *separation ansatz*, which describes the time component of the solution as an exponential function, separating it from the space solution's components $\hat{u}(x)$ and $\hat{p}(x)$:

$$\begin{bmatrix} u(x,t) \\ p(x,t) \end{bmatrix} = e^{\gamma t}\begin{bmatrix} \hat{u}(x) \\ \hat{p}(x) \end{bmatrix}$$

The complex growth rate $\gamma = \sigma + i\omega$ consists of a real growth rate $\sigma = R(\gamma)$ and an angular frequency $\sigma = R(\gamma)$. In general a complex normal mode is either real or appears as conjugated couple of complex numbers. In both cases the physically "real" solution is always the real part of the complex number.

For the space term of the normal mode a complex assumption follows, written in polar coordinates: $\hat{u}(x) = \tilde{u}(x)e^{i\Phi(x)}$ where $\tilde{u}(x) \in R$ is the absolute value and $\Phi(x) \in R$ is the phase.

The disturbance u can thus be rewritten:

$$- \begin{bmatrix} u(x,t) \\ p(x,t) \\ T(x,t) \end{bmatrix} = e^{\gamma t}e^{ik_x x}e^{ik_y y}\begin{bmatrix} \hat{u}(z) \\ \hat{p}(z) \\ \hat{T}(z) \end{bmatrix}$$ in case of the Rayleigh-Bénard problem with k_x

and k_y, the wave number in x and y direction.

$$-\begin{bmatrix} u(x,t) \\ p(x,t) \end{bmatrix} = e^{\gamma t}e^{im\varphi}\begin{bmatrix} \hat{u}(r,z) \\ \hat{p}(r,z) \end{bmatrix}$$ in case of the Taylor-Couette problem with (r, φ, z) as

polar cylindrical coordinates and m as the azimuthal wave number.

For reasons of simplicity we will insert the normal mode ansatz only with time separation into the linear stability equations and generalize for all problems. After the insertion, we obtain:

$$\gamma\hat{u} + U.\nabla\hat{u} + \hat{u}.\nabla U = -\nabla\hat{p} + \frac{1}{Re}\nabla^2\hat{u}$$

$$\nabla.\hat{u} = 0$$

With fixed or periodical boundary conditions for $\tilde{u}(x)$.

The stability equation turns into an eigenvalue problem, which eigenvalues γ and belonging eigenvectors $(\hat{u},\hat{p})$. Existence of symmetry and periodicity in the solution, observed through experiments, can be translated into mathematical relations, which strongly simplify the equations.

Using numerical methods such as the shooting method or the one of the matrix methods (spectral, finite difference, etc) we will compute for a set of parameters (for example Re, phi(x)) the eigenvalues' spectrum of the equation of the form:

$$\gamma A.B = B.X$$

with A, B ∈ Rⁿ x Rⁿ are 2 real matrices and $X = (\hat{u},\hat{p})$i the unknowns' discrete values at the nodes of the domain.

Let's observe a few possibilities:

If $\Im(\gamma) = \pm\omega \neq 0$, than 2 counter circulating waves propagates through the domain.

If $\Im(\gamma) = 0$, than the waves behave exponentially and no more oscillatory.

Depending on the sign of $\Re(\gamma)$ we reach different states, which are:

$$\left.\begin{array}{l} linear\ stabil \\ neutral\ stabil \\ linear\ instabil \end{array}\right\} \Leftrightarrow \max\sigma_n \left\{\begin{array}{l} < 0, \\ = 0, \\ > 0. \end{array}\right.$$

3.2   Bifurcation and pattern classification

A bifurcation is a sudden 'qualitative' or topological change in the behaviour of a system occurring when a small smooth change is made to the parameter values (the bifurcation parameters) of that system. It is a strong evidence for crossing into instability.
The parameter value, at which it occurs, is called "critical parameter" or "critical point"
The demonstration of bifurcation can be made with help of the Taylor-Couette problem.
That is, we want in this case to draw a 2D-graph with a *control parameter*, a parameter we can experimentally vary at will, on the horizontal axe and an *order parameter*, a fluid flow variable we can measure. Such a flow variable needs to be one, which drastically changes with the transition to instability.

Now let's observe the stable state of our experiment. The Couette-flow remains unchanged along its rotational axe and thus shows a high degree of translational invariance, called continuous translational invariance along the hole cylinder height (see Figure 9a).

The fluid flow velocity measured at any point of the domain remains 0 in the axe direction ($w=0$).

A steady raise of angular velocity yields at a certain value, a critical value, to the formation of Taylor vortices (see Figure 9b). The flow shows a periodical change along its rotational axe and is called discrete translational invariant along L. The fluid flow velocity at the measurement point shows now a nonzero value, which increases with the angular velocity.

The representation on a diagram of the velocity w in axe direction in terms of angular velocity is called a *bifurcation diagram* (see Figure 10) and reveals the critical velocity for transition (Ω_{1c}). The control parameter is the angular velocity Ω_1 and the order parameter is the axial velocity w.
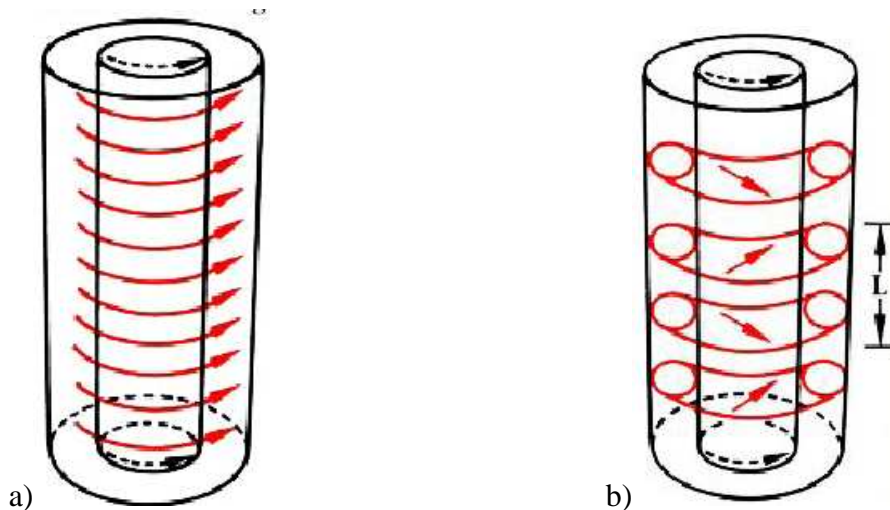
a)   b)
Figure 9: Couette flow (a) and Taylor vortex flow (b) [18]

The critical Reynolds number and its related wave number have been computed through out the literature using different numerical approaches for different ratio of radii. Recktenwald et al. have obtained to following here shortened table:

Radii ratio	0.975	0.90	0.80	0.70	0.60	0.50
Re_crit	260.9	131.6	94.7	79.5	71.7	68.2
k_crit	3.13	3.13	3.13	3.14	3.15	3.16

Table 1: Critical wave and Reynolds numbers for different radii ratios
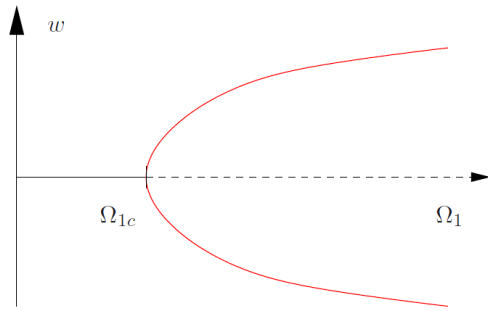
Figure 10: Bifurcation's diagramm of the axial velocity with respect of the angular inner wall velocity. Ω_{1c} is the critical point [5]

If we write a complex eigenvalue near the critical point in its most general form, the occurring unstable mode can be classified according to its eigenvalue.

The general form is: $\gamma(k^2) = i\omega(k^2) + \Lambda(k^2)$ with the real frequency w and the real growth rate Λ, both functions of the wave number k [17].

- For $\omega = 0$ and $\left.\frac{d\Lambda}{dk}\right|_{k=0} = 0$ the instability is spatially *homogeneous* and <u>monoton</u> in time around the critical point. The category name is "*H*<u>m</u>" and the related equation is the real Ginzburg-Landau equation describing for examples gradient systems in physics.

- For $\omega \neq 0$ and $\left.\frac{d\Lambda}{dk}\right|_{k=0} = 0$ the instability is spatially *homogeneous* and <u>oscillating</u> in time around the critical point. The category name is "*H*<u>o</u>" and the related equation is the complex Ginzburg-Landau equation describing for example Hopf-bifurcations.

- For $\omega = 0$ and $\left.\frac{d\Lambda}{dk}\right|_{k=k_c} = 0$ with $k_c \neq 0$ the instability is spatially *periodical* (we call it "*Turing*"), and <u>monoton</u> in time around the critical point. The category name is "*T*<u>m</u>" and requires a system of minimum 2 equations. The related equation is the Swift-Hohenberg equation describing for example Taylor-Couette, convection or Faraday in-stabilities.

- For $\omega \neq 0$ and $\left.\frac{d\Lambda}{dk}\right|_{k=k_c} = 0$ with $k_c \neq 0$ the instability shows a spatial "*Turing*"-structure while <u>oscillating</u> in time around the critical point. The category name is "*T*<u>o</u>" and requires a system of minimum 3 equations. The related equation is the Swift-Hohenberg equation describing for example wave instabilities and some convection instabilities of binary mixtures.

- Furthermore there is a category named *K0* related to the Cahn-Hilliard equation for the description of thin film and Kelvin-Helmholtz instabilities.

A graph of the real part of the eigenvalue with respect to the wave number for the different bifurcation families (Type *H*, Type *T* and Type *K0*), each at different *control parameters* can be seen in Figure 11 with ε = current control parameter – critical control parameter.

Through analysis of the Taylor-Couette problem in this work, we expect the results of our numerical solution to match the type *H*
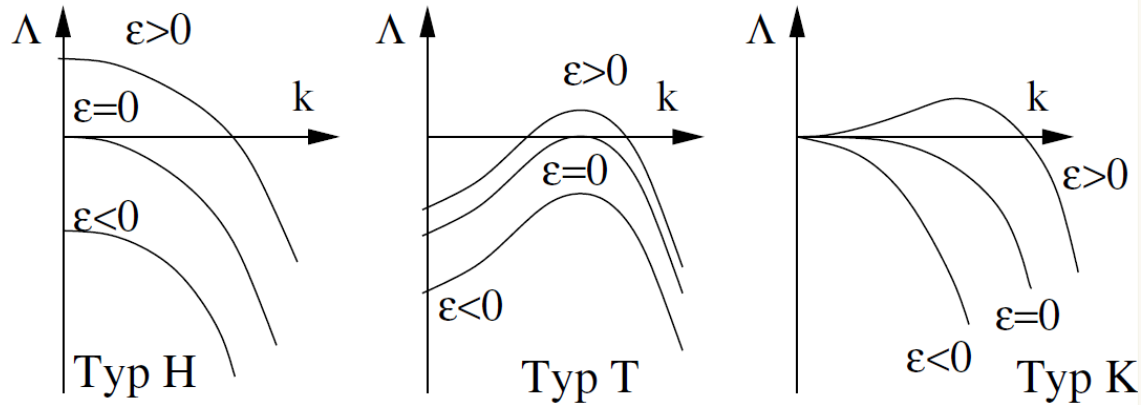
Figure 11: Real part of eigenvalue with respect to the wave number for different bifurcation types [17]

3.3   Application on the Taylor-Couette problem

We start with the usual NS equations in dimensionless form:

$$\frac{\partial U}{\partial t} + U.\nabla U = -\nabla p + \upsilon \nabla^2 U$$

We then add a disturbance u to the basic state U_o and obtain:

$$\frac{\partial u}{\partial t} + U_0.\nabla u + u.\nabla U_0 = -\nabla p + \frac{1}{Re}\nabla^2 u.$$

From the symmetry properties of the basic flow, which are the translational invariance $\left(\frac{d}{dz} = 0\right)$, the rotation invariance $\left(\frac{d}{d\varphi} = 0\right)$ and the time invariance $\left(\frac{d}{dt} = 0\right)$ only the translational invariance in a discrete form (periodicity in axial direction) remains. We, thus, consider axisymmetric disturbances, we can decompose u as:

$$u = v\hat{e}_\phi + \nabla \times \left(\psi \hat{e}_\phi\right)$$

This automatically enforces incompressibility by fulfilling the continuity equation.

For the velocity components we apply the normal mode separation ansatz of the form:

$$v = v(r)e^{ikz}e^{\sigma t}, \quad \psi = \psi(r)e^{ikz}e^{\sigma t}$$

This ansatz supposes a sinusoidal variation of the disturbance in the z-direction with axial wave number *k (k ϵ R)*, a growth rate or amplification factor σ *(σ ϵ C)* for the dis-

turbance, and amplitudes of the disturbance [v(r) and ψ(r)], which are dependent on the radial position.

The (Φ) component of (*) and rot (*) now become [8]:

$$\sigma v = Re^{-1} D^2 v + ikr^{-1} (\Omega r^2)' \psi$$

$$\sigma D^2 \psi = Re^{-1} (D^2)^2 \psi - 2ik\Omega v$$

with the associated boundary conditions:

$$v = \psi = \psi' = 0 \text{ at } r = r_i, r_o$$

And the operators:

$$D^2 = \nabla^2 - \frac{1}{r^2} = \frac{1}{r} \frac{\partial}{\partial r} \left(r \frac{\partial}{\partial r} \right) - \frac{1}{r^2} - k^2$$

(') denotes $\frac{d}{dr}$

A dimensionalization of the system of equations is carried through replacement of 1/Re by ν. So the parameter terms can be inserted in SI unit and the computed terms are collected in SI unit as well. This choice of suppressing the dimensionless Reynolds number from the equations let the angular velocity as direct control parameter, from which the related Reynolds number can be computed, if wanted.

It leads to an eigenvalue problem with σ being the eigenvalue to be determined and Ω(r), Re (through the boundary angular velocity Ω_i) and k being the input parameters. The computed eigenvalues will predict the growth or decay rate of the mode.

The numerical procedure to be developed enables a stability test from a basic state (a given Ω(r) profile) and finding the smallest value that yields to instability (eigenvalue with positive real part). Since the combination of a given Ω(r) and Re is stable only if it is stable for all wavenumbers k, a scan over a broad range of k for a given boundary angular velocity Ω_i is necessary.

We will, thus, gradually increase Re, through increasing Ω_i and vary for each Ω_i the axial wave number k over a broad range until a positive real eigenvalue occurs.

The tested velocity profile originates from the solving of the cylindrical NS equations under the assumption related to the "Couette flow". The occurring differential equations system leads to the basic state velocity profile:

$$\Omega(r) = U_\phi / r = A + B/r^2$$

With :

$$A = \frac{\Omega_o r_o^2 - \Omega_i r_i^2}{r_o^2 - r_i^2} \qquad B = \frac{r_o^2 - r_i^2}{r_o^2 - r_i^2} \left(\Omega_i - \Omega_o \right)$$

This eigenvalue system of equations will be solved numerically using a class of techniques known for its fast convergence. It is the spectral method with Chebyshev polynomials.

4   Spectral method for numerical solving

Spectral methods are a family of methods used in applied mathematics and scientific computing for solving numerically PDEs. In order to find an approximation to the unknown solution, the methods utilize approximations defined in terms of truncated series expansions of orthogonal polynomials (Lagrange, Legendre or Chebyshev) or trigonometric functions (Fourier), substitute the unknows of the PDE with these series and compute the residual of the approximation using either the Galerkin approach or the collocation approach.

<u>Galerkin Approach:</u>

In the Galerkin approach the approximation need to be found so that the residual is orthogonal to the origin space of the unknown, that is to each of the basis functions. Mathematically it means that the integral of the residual-basis function product over the domain must vanish. The following example shows the application:

Consider the PDE: $\frac{\partial u(x,t)}{\partial t} = \frac{\partial u(x,t)}{\partial x}$.

We choose the following approximation: $u_N(x,t) = \sum_{k=-N}^{N} a_j(t) e^{ijx}$.

We define the residual: $R_N = \frac{\partial u_N(x,t)}{\partial t} - \frac{\partial u_N(x,t)}{\partial x}$

We require that:

$$\int_{-\pi}^{\pi} R_N\, e^{-ijx}\, dx = \int_{-\pi}^{\pi} \left(\frac{\partial u_N(x,t)}{\partial t} - \frac{\partial u_N(x,t)}{\partial x} \right) e^{-ijx} dx = 0$$

It leads to:

$$\int_{-\pi}^{\pi} \left(\frac{\partial u_N(x,t)}{\partial t} - \frac{\partial u_N(x,t)}{\partial x} \right) e^{-ijx} dx = \int_{-\pi}^{\pi} \sum_{k=-N}^{N} \left(a_k'(t) e^{-ikx} - ik a_k(t) e^{ikx} \right) e^{ijx} dx$$

$$= \left(a_j'(t) - ij a_j(t) \right) = 0$$

For $-N \leq j \leq N$. Here $a_j'(t)$ denotes the derivative of $a_j(t)$ with respect to time t

To obtain the Galerkin approximation $u_N(x,t)$ we need to solve the ODE

$\frac{da_j(t)}{dt} = ij a_j(t)$ for the coefficients $a_j(t)$. In this case we can do this analytically, of course, but in general we do this using some ODE solver.

Collocation approach:

For the collocation approach this residual has to be computed at a set of domain points, which number equals the number of undetermined coefficients of my series. These points are called "collocation points". The residual equation is required to vanish at those points, which turns the differential equation into a matrix equation. This method is also called "pseudospectral approach"

As example we choose the linear, one-dimensional boundary value problem:

$$u_{xx} - (x^6 + 3x^2)u = 0$$

$$u(-1) = u(1) = 1$$

In order to satisfy the boundary conditions independently of the unknown spectral coefficients, it is convenient to write the approximation as

$u_2 := 1 + (1 - x^2)(a_0 + a_1 x + a_2 x^2)$, where the decision to keep only three degrees of freedom is arbitrary.

The residual for this approximation is: $R(x; a_0, a_1, a_2) = u_{2,xx} - (x^6 + 3x^2)u_2$

and yields:

$$R = (2a_2 + 2a_0) - 6a_1 x - (3 + 3a_0 + 12a_2)x^2 - 3a_1 x^3 + 3(a_0 - a_2)x^4 + 3a_1 x^5$$
$$+ (-1 - a_0 + 3a_2)x^6 - a_1 x^7 + (a_0 - a_2)x^8 + a_1 x^9 + 10a_2 x^{10}$$

To minimize the approximation error, we choose to make the residual zero at a set of points (collocation points) equal in number to the undetermined coefficients in u2(x). Let's arbitrarily choose the points xi = (-1/2; 0; 1/2), we obtain the three equations:

$$eq1 = -\frac{659}{256}a_0 + \frac{1683}{512}a_1 - \frac{1171}{1024}a_2 - \frac{49}{64}$$

$$eq2 = -2(a_0 - a_2)$$

$$eq3 = -\frac{659}{256}a_0 - \frac{1683}{512}a_1 - \frac{1171}{1024}a_2 - \frac{49}{64}$$

The coefficients are then determined by solving $eq1 = eq2 = eq3 = 0$ and yields:

$$a_0 = -\frac{784}{3807}, \quad a_1 = 0, \quad a_2 = a_0$$

The solution can be reconstructed by substituting the constants in u2.

Collocation points within the collocation approach:

The first idea we might have is to use equispaced interpolation points. It has turned out to be catastrophically bad in general, because a problem know as "Runge phenomenon" encounters. Discovered by Carl David Tolmé Runge, wenn exploring errors' behaviour by polynomial interpolation of functions, it describes the problem of oscillation at the edges of an interval that occurs when using polynomial interpolation with polynomials of high degree. This phenomenon corresponds to the Gibbs phenomenon in Fourier series approximations (see Figure 12).
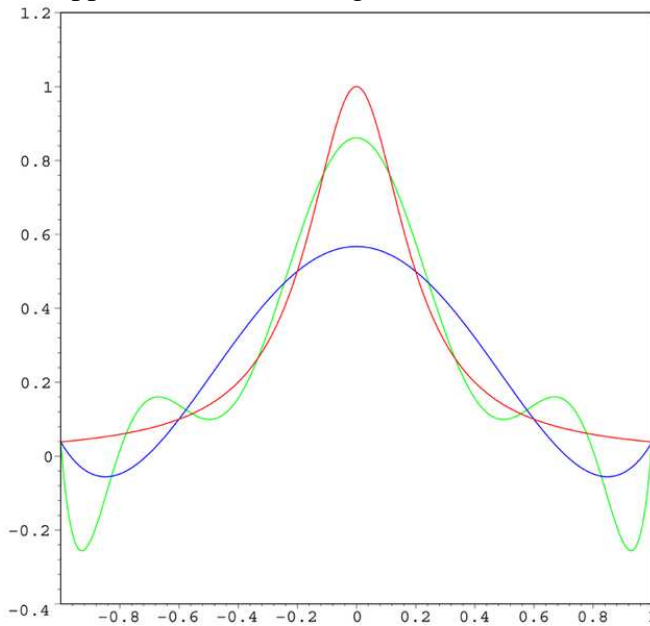

Figure 12: The red curve is the Runge function. The blue curve is a 5th-order interpolating polynomial (using six equally-spaced interpolating points).The green curve is a 9th-order interpolating polynomial (using ten equally-spaced interpolating points)

This means, that for equally spaced points the residuals at the edges not only fail to converge in general with increasing N (degree of polynomial), but the residual even diverges at a rate of up to 2^N.

Optimal interpolation points should therefore be unevenly spaced and yield to a rapid vanishment of the residual.

The solution has been found for the particular case of Lagrangian polynomials and can be applied without restriction to all types of polynomials. It says that the OPTIMAL INTERPOLATION POINTS are the ROOTS of the CHEBYSHEV POLYNOMIAL of DEGREE (N +1) [9]. Although this family of polynomials will be presented in an upcoming chapter, we anticipate in the explanation of "root of Chebyshev polynomials" also named "Chebyshev grid points".

If a semicircle of unit radius is cut into evenly spaced segments, and then vertical lines are drawn from these "Fourier" grid points to the line segment [-1; 1], which is the base of the semicircle, the vertical lines will intersect the horizontal line at the Chebyshev grid points.

The polar coordinates of the grid points on the semicircle are unit radius and angle $\theta = \pi(2i - 1)/(2N)$ where $i = 1,\ldots, N$. The Chebyshev grid points are $x_i = \cos(\theta_i)$.

We derive thus only two optimal sets of interpolation points, the Gauss-Chebyshev points and the Gauss-Lobatto points.

$$x_i = \cos\left[\frac{(2i-1)\pi}{2N}\right] \quad i = 1, ..., N \text{ ["Roots" or "Gauss-Chebyshev"]}$$

$$x_i = \cos\left[\frac{\pi i}{N-1}\right] \quad i = 0, ..., N-1 \text{ ["Extrema-plus-Endpoints or "Gauss-Lobatto"]}$$
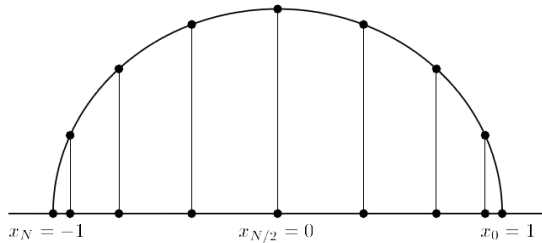
Figure 13: Chebyshev points are projections onto the x-axis of equally spaced points on the unit circle [13]

The use of the Chebyshev points reduces strongly the Runge phenomenon (see Figure 14):
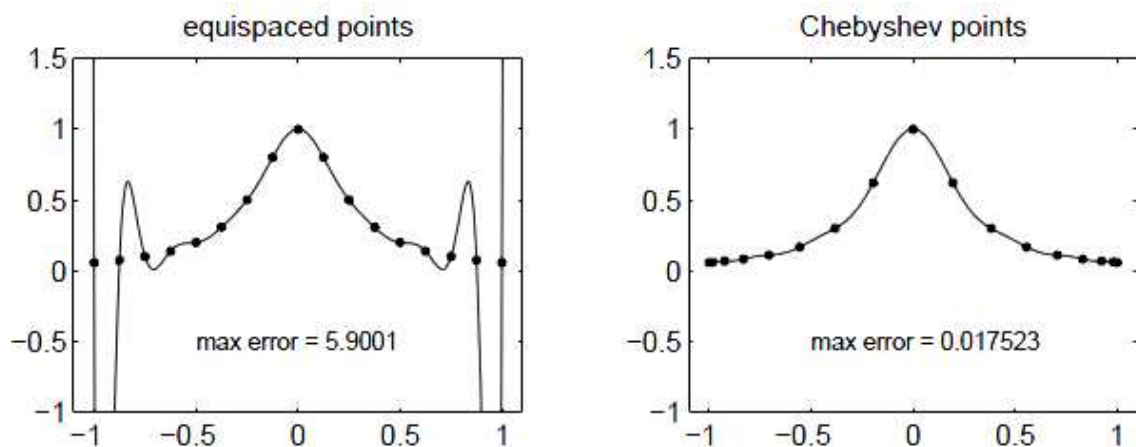
Figure 14: Degree N interpolation of $u(x) = 1/(1 + 16x^2)$ in N+1 equispaced and Chebyshev points. With increasing N, the errors increase exponentially in the equis-paced case (Runge Phenomenon) whereas in the Chebyshev case they decrease exponentially [13]

Both approaches have an excellent, so called "exponential convergence", which is the fastest possible among the numerical techniques [9]. The reason lies in the whole do-main overlapping expansion (global approach) of the approximated solution in compari-son to other algorithm families. Figure compares the regions of direct dependency in derivative formulas for the three families of algorithms, where for the finite difference and finite element methods only those points which lie within a given subdomain con-tribute directly to the derivative approximations in that subdomain (local approach).
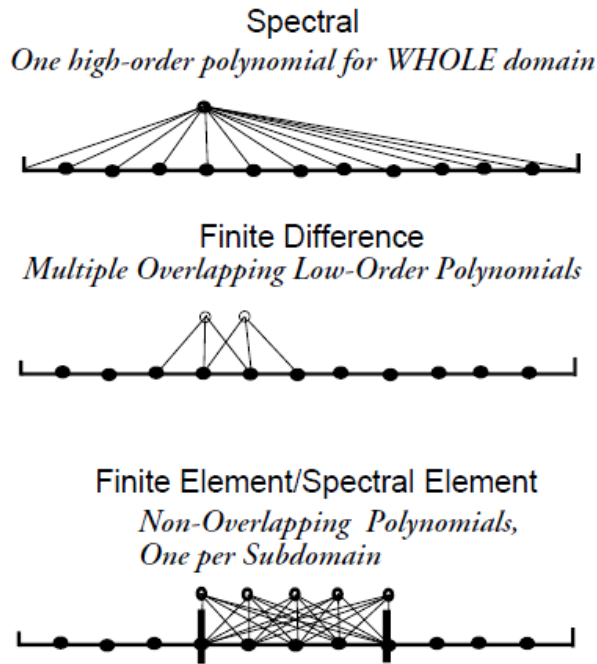
Figure 15: Three types of numerical algorithms. The thin, slanting lines illustrate all the grid points (black circles) that directly affect the estimates of derivatives at the points shown above the lines by open circles. The thick black vertical lines in the bottom grid are the subdomain walls [9]

This global approach requires that the solution to be computed remains smooth over its entire domain for an accurate result (no shock capturing method). Depending on whether a problem is bounded and periodic or bounded and non-periodic, the Fourier series or the polynomial expansion approach is more suitable.

4.1   Chebyshev polynomials

Chebyshev polynomials, named after Pafnuty Chebyshev, are a sequence of recursively defined orthogonal polynomials. Polynomials are orthogonal, when their inner product on the vector space of all polynomials equals zero. One distinguishes between Chebyshev polynomials of first kind (Tn) and of second kind (Un), as well as a pair of related (Jacobi) polynomials, which are called Chebyshev polynomials of third kind (Vn) and of fourth kind (Wn). All these polynomials haven taken an important position in the field of approximation theory, numerical integration and spectral methods for partial differential equations. We will focus on the Chebyshev polynomials of first kind (Tn) to construct spectral methods for our bounded, non-periodic eigenvalue problem.

Chebyshev polynomials Tn(x) of the first kind is a polynomial in x of degree n, defined in the interval [-1, 1] by the recurrence relation:

$$T_0(x) = 1$$

$$T_1(x) = x$$

$$T_{n+1}(x) = 2xT_n(x) - T_{n-1}(x) \quad x \in [-1,1]$$

We show a short list of developed polynomials until degree 9:

$$T_0(x) = 1$$

$$T_1(x) = x$$

$$T_2(x) = 2x^2 - 1$$

$$T_3(x) = 4x^3 - 3x$$

$$T_4(x) = 8x^4 - 8x^2 + 1$$

$$T_5(x) = 16x^5 - 20x^3 + 5x$$

$$T_6(x) = 32x^6 - 48x^4 + 18x^2 - 1$$

$$T_7(x) = 64x^7 - 112x^5 + 56x^3 - 7x$$

$$T_8(x) = 128x^8 - 256x^6 + 160x^4 - 32x^2 + 1$$

$$T_9(x) = 256x^9 - 576x^7 + 432x^5 - 120x^3 + 9x$$
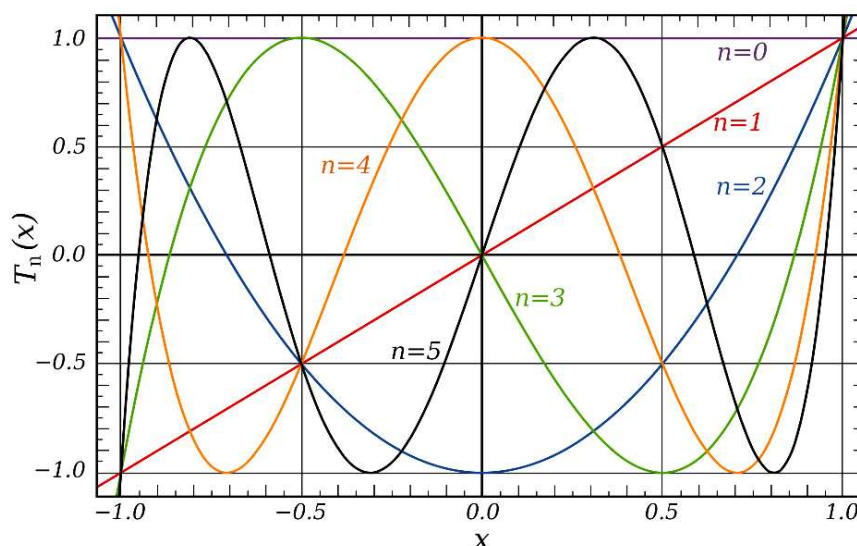
Chebyshev polynomials of degree 0 till 5 in a graph:

Figure 16: The first few Chebyshev polynomials of the first kind in the domain $-1 < x < 1$: The flat T_0, T_1, T_2, T_3, T_4 and T_5.

The necessary orthogonality condition of the polynomial is fulfilled with respect to the weight function: $\frac{1}{\sqrt{1-x^2}}$.

5   Solving the eigenvalue problem

We recall the eigenvalue differential equations system with its boundary conditions

$$\sigma v = Re^{-1}D^2 v + ikr^{-1}(\Omega r^2)' \psi$$

$$\sigma D^2 \psi = Re^{-1}(D^2)^2 \psi - 2ik\Omega v$$

$v = \psi = \psi' = 0$ at $r = r_i, r_0$

We rewrite the equations in matrix form:

$$\sigma \begin{bmatrix} 1 & 0 \\ 0 & D^2 \end{bmatrix} \begin{bmatrix} v \\ \psi \end{bmatrix} = \begin{bmatrix} Re^{-1}D^2 & ikr^{-1}(\Omega r^2)' \\ -2ik\Omega & Re^{-1}(D^2)^2 \end{bmatrix} \begin{bmatrix} v \\ \psi \end{bmatrix}$$

At first we write explicitly:

$$D^2 = \nabla^2 - \frac{1}{r^2} = \frac{1}{r}\frac{\partial}{\partial r}\left(r\frac{\partial}{\partial r}\right) - \frac{1}{r^2} - k^2 = \frac{\partial^2}{\partial r^2} + \frac{1}{r}\frac{\partial}{\partial r} - \frac{1}{r^2} - k^2$$

$$(D^2)^2 = \frac{\partial^4}{\partial r^4} + \frac{2}{r}\frac{\partial^3}{\partial r^3} - \left(\frac{3}{r^2} + 2k^2\right)\frac{\partial^2}{\partial r^2} + \left(\frac{3}{r^3} - \frac{2k^2}{r}\right)\frac{\partial}{\partial r} + \left(\frac{-3}{r^4} + \frac{2k^2}{r^2} + k^4\right)$$

(') denotes $\frac{d}{dr}$

$$\Omega = \Omega(r) = U_\phi/r = A + B/r^2 = \left(\frac{\Omega_0 r_0^2 - \Omega_i r_i^2}{r_0^2 - r_i^2}\right) + \left(\frac{r_0^2 - r_i^2}{r_0^2 - r_i^2}(\Omega_i - \Omega_0)\right)/r^2$$

We expand the unknows (v and ψ) according to the spectral collocation method with Chebyshev polynomials, where N stands for the number of internal points (Roots) to be computed. The number of roots needs to be increased by 2 and 4 respectively for v and ψ according to the number of boundary conditions related to v and ψ.

$$v(r) = \sum_{n=1}^{N+2} v_n T_{n-1}(x) \qquad\qquad \psi(r) = \sum_{n=1}^{N+4} \psi_n T_{n-1}(x)$$

We carry a coordinate transformation within the polynomials from x to r according to the linear transformation: $r = \frac{r_0 + r_i}{2} + x\frac{r_0 - r_i}{2}$ with r ϵ [r$_i$, r$_o$] and x ϵ [−1, 1]. That is, the interval is mapped to the standard interval for the Chebyshev polynomials. Table 3 shows such a transformation applied to polynomials of degree 0 till 5, where $c = \frac{2}{r_0 - r_i}$ and $= \frac{r_0 + r_i}{r_0 - r_i}$, together with their derivatives.

We insert the expanded polynomials into the equations, which yields algebraic equations depending on the coefficients v_i, ψ_i and r.

The collocations points (roots) are developed according to the Gauß-Lobatto-method (see Chapter 20), linearly transformed from *x* to *r* (see Table 2) and truncated from the first and last point (boundary points) before their insertion into the algebraic equations. This step converts the algebraic equation into a $(2N + 2) \times (2N + 2)$ matrix problem.

For the case of N=4 we obtain the system in Figure 17, where for each matrix the rows correspond to the collocation points, the columns to the Chebyshevs T_i and the green rows to the boundary conditions' equations, which are also written as a linear combination of the coefficients v_n and ψ_n.

$$\sigma v = Re^{-1}D^2 v + ikr^{-1}(\Omega r^2)' \psi$$

$$\sigma D^2 \psi = Re^{-1}(D^2)^2 \psi - 2ik\Omega v$$

Figure 17: Eigenvalue problem in matrix form for N=4 with labelled submatrices [8]

We remind here, that a dimentionalization of the system is carried as mentioned in chapter 3.3 (underlined passage).

	x_j	r_j		x_j	r_j
T_0	0	a	T_4	-1 $-\sqrt{2}/2$ 0 $\sqrt{2}/2$ 1	$a - b$ $a - b\sqrt{2}/2$ a $a + b\sqrt{2}/2$ 1
T_1	-1 $+1$	$a - b$ $a + b$			
T_2	-1 0 1	$a - b$ a $a + b$	T_5	-1 -0.809 -0.309 0.309 0.809 1	$a - b$ $a - 0.809b$ $a - 0.309b$ $a + 0.309b$ $a + 0.809b/2$ $a + b$
T_3	-1 -0.5 0.5 1	$a - b$ $a - b/2$ $a + b/2$ $a + b$			

Table 2: Non-truncated Gauß-Lobatto collocation points related to the grade of the polynomial *before* and *after* linear transformation with a=(r$_o$+r$_i$)/2 and b=(r$_o$-r$_i$)/2

	$T(x)$	$T(r)$	$\frac{\partial}{\partial r} T(r)$	$\frac{\partial^2}{\partial r^2} T(r)$	$\frac{\partial^3}{\partial r^3} T(r)$	$\frac{\partial^4}{\partial r^4} T(r)$
T_0	1	1	0	0	0	0
T_1	x	$cr - e$	c	0	0	0
T_2	$2x^2 - 1$	$2(cr - e)^2 - 1$	$4c(cr - e)$	$4c^2$	0	0
T_3	$4x^3 - 3x$	$4(cr - e)^3 - 3(c$	$12c(cr - e)^2 - 3c$	$24c^2(cr - e)$	$24c^3$	0
T_4	$8x^4 - 8x^2 + 1$	$8(cr - e)^4 - 8(c$	$32c(cr - e)^3 - 16$	$96c^2(cr - e)^2 - 16$	$192c^3(cr - e)$	$192c^4$
T_5	$16x^5 - 20x^3 +$	$16(cr - e)^5 - 20$	$80c(cr - e)^4 - 60$	$320c^2(cr - e)^3 - 6$	$960c^3(cr - e)^2 -$	$1920c^4(cr - e)$

Table 3: The first few Chebyshev polynomials in their original form ($T(x)$, x ∈ [−1, 1]) and after the coordinate transformation ($T(r)$, r ∈ [r_i, r_o]) with the belonging derivatives.

6 Numerical set-up

The MATLAB environment has been used for computation, where a series of functions have been implemented to support the main program.

Function ChebT(N): computes the coefficients of the Nth Chebyshev polynomial of the first kind. These coefficients are stored in the descending order of powers (see Table 4).

Chebyshev polynomials	ChebT(N)-results
$T_0(x) = 1$	[1]
$T_1(x) = x$	[1 0]
$T_2(x) = 2x^2 - 1$	[2 0 -1]
$T_3(x) = 4x^3 - 3x$	[4 0 -3 0]
$T_4(x) = 8x^4 - 8x^2 + 1$	[8 0 -8 0 1]
$T_5(x) = 16x^5 - 20x^3 + 5x$	[16 0 -20 0 5 0]

Table 4: Results of function ChebT(N) in comparison to few Chebyshev polynomials

Function Subst_D(N, r_i, r_o): uses the coefficients of *ChebT(N)* to build the Nth Chebyshev polynomial T(x) with help of the MATLAB-Symbolic-toolbox. It, then, substitutes the x-variable with the r-variable using the linear relationship between x and r. The linear equation is: $x = cr - e = \frac{2}{r_o - r_i} r - \frac{r_o + r_i}{r_o - r_i}$ and the results for a few Chebyshev polynomials with $r_i = 0.8$ and $r_o = 1$ can be seen in Table 5.

Chebyshev polynomials	Re_Subst_D(N,0.8,1)-results
$T_0(x) = 1$	$T_0(r) = 1$
$T_1(x) = x$	$T_1(r) = 10r - 9$
$T_2(x) = 2x^2 - 1$	$T_2(r) = 200r^2 - 360r + 161$
$T_3(x) = 4x^3 - 3x$	$T_3(r) = 4000r^3 - 10800r^2 + 9690r - 2889$
$T_4(x) = 8x^4 - 8x^2 + 1$	$T_4(r) = 80000r^4 - 288000r^3 + 388000r^2 - 231840r + 518$
$T_5(x) = 16x^5 - 20x^3$	$T_5(r) = 1.6e^6 r^5 - 7.2e^6 r^4 + 12.94e^6 r^3 - 11.61e^6 r^2 + 5200$

Table 5: Results of function Re_Subst_D(N,0.8,1) in comparison to few Chebyshev polynomials

Main program:

The main program computes meanwhile the x-collocation-vector after Gauß-Lobatto using the input "N", truncates and transforms this vector into the r- collocation-vector.

In the MATLAB environment it looks like this:

```
x = -cos(pi*(0:n+1)/(n+1));   % Computation of the x-collocation points
x = x(2:n+1);                 % Truncation to lose the boundary points
r_a = x*(b-a)/2 + (b+a)/2;    % Transformation into r-collocation points
```

Keeping r_i=0.8 (here "a") and r_o=1 (here "b") and considering N=5, the points computed with the those MATLAB lines are respectively:

x = -1.0000   -0.8660   -0.5000   0.0000   0.5000   0.8660   1.0000

x = 0.8660   0.5000   0.0000   -0.5000   -0.8660

r_a = 0.8134   0.8500   0.9000   0.9500   0.9866

A loop is conceived, so that the function *Subst_D(N, r_i , r_o)* computes the $T_j(r)$-polynomials in ascending order. We substitute for each new polynomial the unknown "r" of the polynomial by the vector "r_a" and store the row vector in a dynamic matrix. In order to keep the matrix quadratic, we need to extend the vector "r_a" according to the requirement of the series. That means an addition of 2 elements for series of *v* and an addition of 4 elements for the series of ψ. We, then, have:

- r_a_v = 0.8134   0.8500   0.9000   0.9500   0.9866   0   0
- r_a_ψ = 0.8134   0.8500   0.9000   0.9500   0.9866   0   0   0   0

If we keep N = 5, we thus obtain for each of the unknowns of the differential equation the Chebyshev-matrix:

$$v(r) = \sum_{n=1}^{N+2} v_n T_{n-1}(r) = \begin{pmatrix} T_0(0.8134) & \cdots & T_6(0.8134) \\ \vdots & \ddots & \vdots \\ T_0(0) & \cdots & T_6(0) \end{pmatrix} \begin{pmatrix} v_1 \\ \vdots \\ v_7 \end{pmatrix}$$

$$\psi(r) = \sum_{n=1}^{N+4} \psi_n T_{n-1}(r) = \begin{pmatrix} T_0(0.8134) & \cdots & T_8(0.8134) \\ \vdots & \ddots & \vdots \\ T_0(0) & \cdots & T_8(0) \end{pmatrix} \begin{pmatrix} \psi_1 \\ \vdots \\ \psi_9 \end{pmatrix}$$

Staying in the same logic, a differentiation of the unknows would simply mean:

$$\frac{\partial}{\partial r} v(r) = \sum_{n=1}^{N+2} v_n \frac{\partial}{\partial r}[T_{n-1}(r)] = \begin{pmatrix} \frac{\partial}{\partial r}[T_0(r)]_{r=0.8134} & \cdots & \frac{\partial}{\partial r}[T_6(r)]_{r=0.8134} \\ \vdots & \ddots & \vdots \\ \frac{\partial}{\partial r}[T_0(r)]_{r=0} & \cdots & \frac{\partial}{\partial r}[T_6(r)]_{r=0} \end{pmatrix} \begin{pmatrix} v_1 \\ \vdots \\ v_7 \end{pmatrix}$$

$$\frac{\partial}{\partial r}\psi(r) = \sum_{n=1}^{N+2} \psi_n \frac{\partial}{\partial r}[T_{n-1}(r)]$$

$$= \begin{pmatrix} \frac{\partial}{\partial r}[T_0(r)]_{r=0.8134} & \cdots & \frac{\partial}{\partial r}[T_8(r)]_{r=0.8134} \\ \vdots & \ddots & \vdots \\ \frac{\partial}{\partial r}[T_0(r)]_{r=0} & \cdots & \frac{\partial}{\partial r}[T_8(r)]_{r=0} \end{pmatrix} \begin{pmatrix} \psi_1 \\ \vdots \\ \psi_9 \end{pmatrix}$$

which by usage of for example the operators

$$D^2 = \frac{\partial^2}{\partial r^2} + \frac{1}{r}\frac{\partial}{\partial r} - \frac{1}{r^2} - k^2$$

on the unknown v leads to the conclusion:

$$D^2 v(r) = \sum_{n=1}^{N+2} v_n D^2[T_{n-1}(r)] = \begin{pmatrix} D^2[T_0(r)]_{r=0.8134} & \cdots & D^2[T_6(r)]_{r=0.8134} \\ \vdots & \ddots & \vdots \\ D^2[T_0(r)]_{r=0} & \cdots & D^2[T_6(r)]_{r=0} \end{pmatrix} \begin{pmatrix} v_1 \\ \vdots \\ v_7 \end{pmatrix}$$

$$= \left(\begin{pmatrix} \frac{\partial^2}{\partial r^2}[T_0(r)]_{r=0.8134} & \cdots & \frac{\partial^2}{\partial r^2}[T_6(r)]_{r=0.8134} \\ \vdots & \ddots & \vdots \\ \frac{\partial^2}{\partial r^2}[T_0(r)]_{r=0} & \cdots & \frac{\partial^2}{\partial r^2}[T_6(r)]_{r=0} \end{pmatrix} \right.$$

$$+ \begin{pmatrix} \left[\frac{1}{r}\frac{\partial}{\partial r}T_0(r)\right]_{r=0.8134} & \cdots & \left[\frac{1}{r}\frac{\partial}{\partial r}T_6(r)\right]_{r=0.8134} \\ \vdots & \ddots & \vdots \\ \left[\frac{1}{r}\frac{\partial}{\partial r}T_0(r)\right]_{r=0} & \cdots & \left[\frac{1}{r}\frac{\partial}{\partial r}T_6(r)\right]_{r=0} \end{pmatrix}$$

$$- \begin{pmatrix} \left[\frac{1}{r^2}T_0(r)\right]_{r=0.8134} & \cdots & \left[\frac{1}{r^2}T_6(r)\right]_{r=0.8134} \\ \vdots & \ddots & \vdots \\ \left[\frac{1}{r^2}T_0(r)\right]_{r=0} & \cdots & \left[\frac{1}{r^2}T_6(r)\right]_{r=0} \end{pmatrix}$$

$$\left. - \begin{pmatrix} k^2 & \cdots & k^2 \\ \vdots & \ddots & \vdots \\ k^2 & \cdots & k^2 \end{pmatrix} \right) \begin{pmatrix} v_1 \\ \vdots \\ v_7 \end{pmatrix}$$

Because we start with the $T_j(r)$-polynomial (result of the function *Subst_D(N, r_i, r_o)*) we can easily compute the differentiation matrices of any order by differentiating the polynomial to the required order and substituting the unknown "r" with the extended vector "r_a", as previously done for the Chebyshev matrix.

Adding the boundary conditions to the equations requires the overwriting of the 2 extended rows of *v(r)* with the 2 equations:

$$v(r_i) = \sum_{n=1}^{N+2} v_n T_{n-1}(r_i) = 0 \qquad and \qquad v(r_o) = \sum_{n=1}^{N+2} v_n T_{n-1}(r_o) = 0$$

and the overwriting of the 4 extended rows of *ψ(r)* with the 4 equations:

$$\psi(r_i) = \sum_{n=1}^{N+4} v_n T_{n-1}(r_i) = 0 \qquad and \qquad \psi(r_o) = \sum_{n=1}^{N+4} v_n T_{n-1}(r_o) = 0$$

$$\frac{\partial}{\partial r}\psi(r_i) = \sum_{n=1}^{N+4} v_n \frac{\partial}{\partial r}T_{n-1}(r_i) = 0 \qquad and \qquad \frac{\partial}{\partial r}\psi(r_o) = \sum_{n=1}^{N+4} v_n \frac{\partial}{\partial r}T_{n-1}(r_o) = 0$$

We then rebuild our matrices according to Figure 1Figure 17 an use the built-in "eig"-function of MATLAB to obtain the eigenvalues of the system for the chosen rotational frequency of the inner wall Ω_i and k the chosen wave number. One question remains:

If we discretize the system with the amount N of inner collocation points for each of the unknows, we obtain an eigenvalue vector with (2*N+6) elements. Which eigenvalues are "real-existent" and which are "artefact"?

N=3	N=4	N = 5
61,25481109	264,8349055	630,457737
41,38233975	154,0798383	556,828054
	-	-
-41,88030239	81,79466514	239,678155
	-	-
-25,36682377	108,4525213	200,327503
8,06618E-14	2,1325E-11	4,1687E-10
		-
-2,66276729	-2,7170386	44,1332341
		-
-8,963157049	9,988425828	2,70708263
		-
-1,9015E-12	-12,2970891	21,8420432
		-
-6,6572E-15	18,83656199	26,8901804
		-
-5,17022E-15	5,01191E-12	10,5500427
	-1,51748E-13	-
-4,8931E-16		10,7859461
		-2,8273E-11
0	-1,7884E-13	-1,1298E-13
	3,84253E-15	3,3872E-13
	0	2,4686E-17
		0

Artefact-eigenvalues

Table 6: Eigenvalues for different collocation numbers. The artefacts are coloured.

The artefact-eigenvalues have the property to be smaller than 10^{-6} (absolute value) and are exactly 6 in number (see Table 6). This number corresponds to the number of boundary conditions added to the equations for internal points. Their analytical value is 0. Therefore a filter λ has been built in, which goes through the computed eigenvalues and erases the values between $-\lambda$ and $+\lambda$. The filter value can be set at will.

6.1   Simulation and results

The main goal of this simulation is to find at which collocation number N the critical values for the input parameter (here the rotational velocity of the inner wall) match with the literature values. A study had been carried for N=1 (we refer to [19]) and brought the following result:

	Reynolds number (Re)	Wave number (k)
Literature values	94.7	15.65
Computed values for N =1	87.44	13.7
Residual	7.26	1.95

Table 7: Comparison between literature values and computed values of the critical Reynolds number and related wave number for N = 1

To roughly localize the critical velocity with its related wave number, a first simulation will be carried out with generously broad ranges for the wave number and near-critical-Re ranges for the Reynolds number. The following simulation parameters have been implemented in SI units:

- Inner radius 0.8 [m] and Outer radius = 1 [m].

- Gap width = 0.2 [m].

- Fluid viscosity $\nu = 1$ [m^2/s].

- Inner radius frequency related Reynolds number Re = [92, 96] with an incremental step size of 1.

- Wave number k = [0.5, 25] with an incremental step size of 1.

- Number of inner points N = 5.

- Artefact-Filter $\lambda = 10^{-2}$

The computed diagrams are:

-   real part of maximal eigenvalue over wavenumber for each Reynolds number and

-   maximum of the real part of maximal eigenvalue over Reynolds number

Those should be compared with literature together with the resulting critical wavenumber, Reynolds number, at which the maximal eigenvalue turns positive (the fluid flow becomes unstable).

6.1.1 Maximal eigenvalue-wave number diagram for N = 5

The following diagram shows for Reynolds numbers between 85 and 100 a similar curve shape of the maximal real eigenvalue with respect to the wave number. We increase Re by 1 every loop and obtain 20 curves.
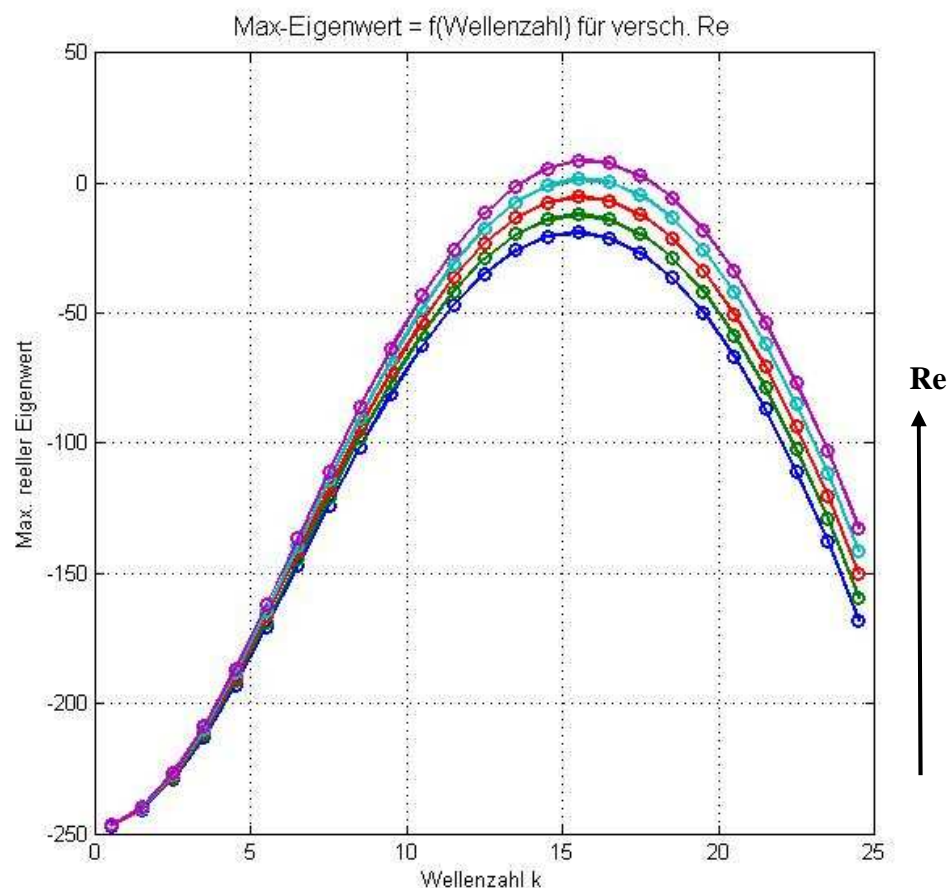

Figure 18: Maximal real eigenvalue with respect to the wave number for different Reynolds number (92≤Re≤96)

We recall the expected qualitative graphs for the problems' family, to which the Taylor-Couette instability belongs (see Figure 19). We conclude that the computed graph shapes show similarities with the theoretical ones. The critical values are reached as soon as the curve is tangent to the x-axe. That is, for the Reynolds number as control parameter, ε = current Re – critical Re. This occurs for Re between 87 and 88.

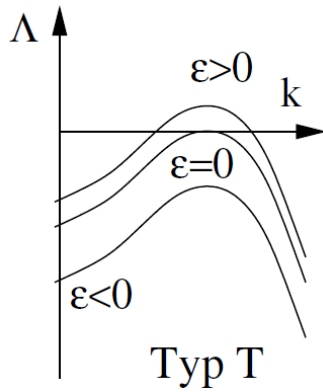Figure 19: Theoretical maximal eigenvalue-wave number graphs of type "Turing"

The related wave number lies between 15 and 17.

A range refinement of the 2 control variables between [94, 95] for Re and [15, 17] for k would bring accurate results.

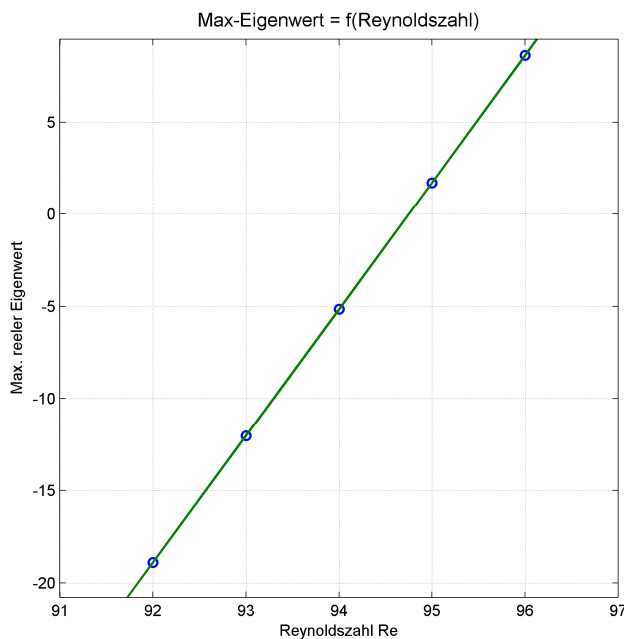### 6.1.2 Maximal real eigenvalue-Reynolds number diagram for N = 5

Figure 20: Maximum of the maximal real eigenvalue with respect to the Reynolds number

If we plot the maximum of each curve from figure over its respective Reynolds number, we obtain the maximum of maximal eigenvalue with respect to Re. It shows a linear relation between the two terms with a slope of 5.7267871. It allows a linear interpolation for the computation of the exact critical Reynolds number for Max-eigenvalue = 0.

	Reynolds number (Re)	Maximal real eigenvalue
	94.0000000000000	-5.15581706639940
	95.0000000000000	1.72633064234536
Linear interpolation	94.7491582	0

Table 8: Linear interpolation for the critical point

The critical Reynolds number is, thus, 94.75.

This number confirms the readjustment of our range for Re from [92, 96] to [94, 95], in order to obtain the related wave number. A scan within the latter range would confirm the critical value of Re, forcing a comparison between the graphical critical number with the interpolated one and at the same time give the related wave number.

6.1.3 Maximal eigenvalue-wave number diagram for N = 5 (revisited)

For Re [94, 95] with a step size of 0.1 and k [15, 17] with a step size of 0.1, we obtain the diagram of Figure 21. The curves shows, that the critical Re lies between 94.7 (fourth curve from the highest) and 94.8 (third curve from the highest) which complies with the interpolated value 94.75. The corresponding wave number k =15.7.
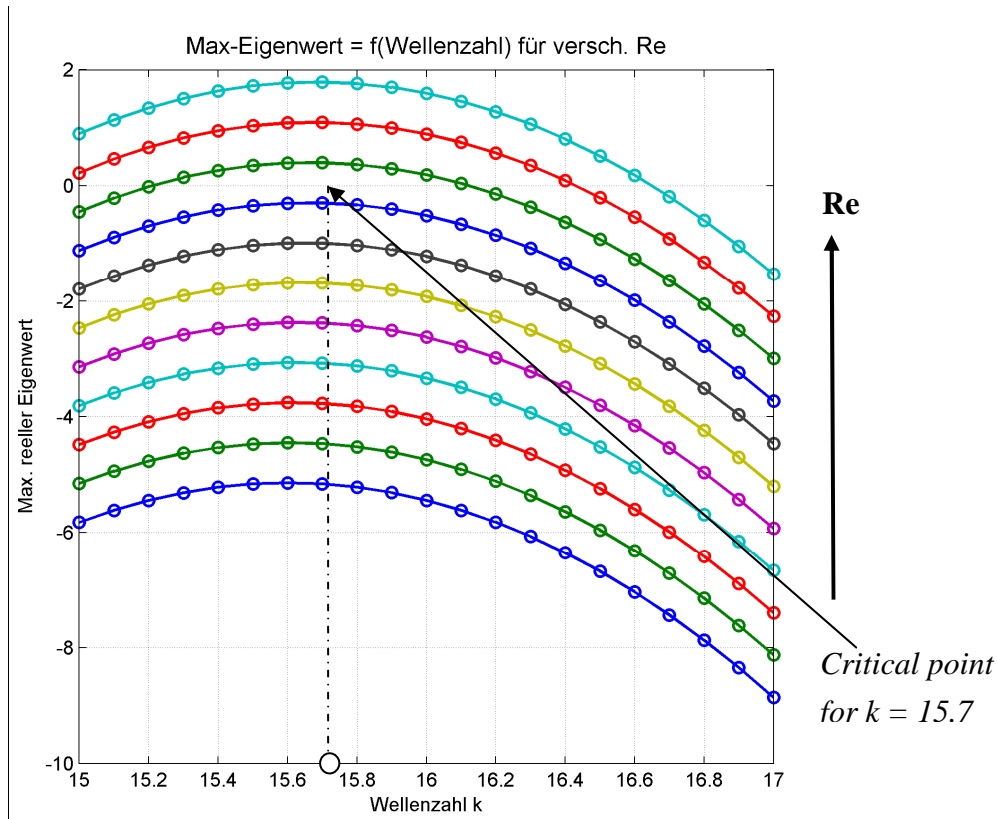
Figure 21: Truncated diagram of the maximal real eigenvalue with respect to the wave number for different Reynolds number for N = 5

6.1.4 Critical values of the Reynoldsnumber for N > 5 and Runge phenomenon

We assume that with increasing number of collocation points (N), the accuracy of the critical Reynolds number (Re) increases. Simultaneously the simulation time increases rapidly with N. Instead of varying Re and scanning over multiple wave numbers (k), we will fix Re = 94.7 and k = 15.65, which are the critical values in the literature, and vary N (N= 10, 20, 30....)

Table 9 shows for different N the maximum of the real-eigenvalues. These eigenvalues increase rapidly with N, which is proof of the Runge phenomenon. The challenge in the use of Chebyshev polynomials is to choose the number of collocation points, so that this effect doesn't occur.

N	10	20	30	40	50	60
real(σ)	-0.2331	-0.2441	-0.0346	0.1672	4.3e07	2.8e08

Table 9: Real eigenvalues with respect to collocation number at the critical point (Re=94.7; k=15.65)

6.1.5 Influence of the position of the collocation points

As mentioned earlier the collocation points are computed after Gauß-Lobatto (see Figure 13 and Chapter 6/main programm). We are interested in the influence of uniformly distributed points on the results. Therefore we compare the results of a simulation based on the values of chapter 6.1.3 (Re [94, 95] with a step size of 0.1 and k [15, 17] with a step size of 0.1) for N=5 but equally spaced.

Figure 22 shows extremely high maximal real eigenvalue compared to Figure 13. This wrong solution confirms the theoretical approach, which predicts accurate results through usage of Chebyshev polynomials only and only if the collocation points are the Gauß-Chebyshev or the Gauß-Lobatto points. Explanations can be read in [9, p.3]
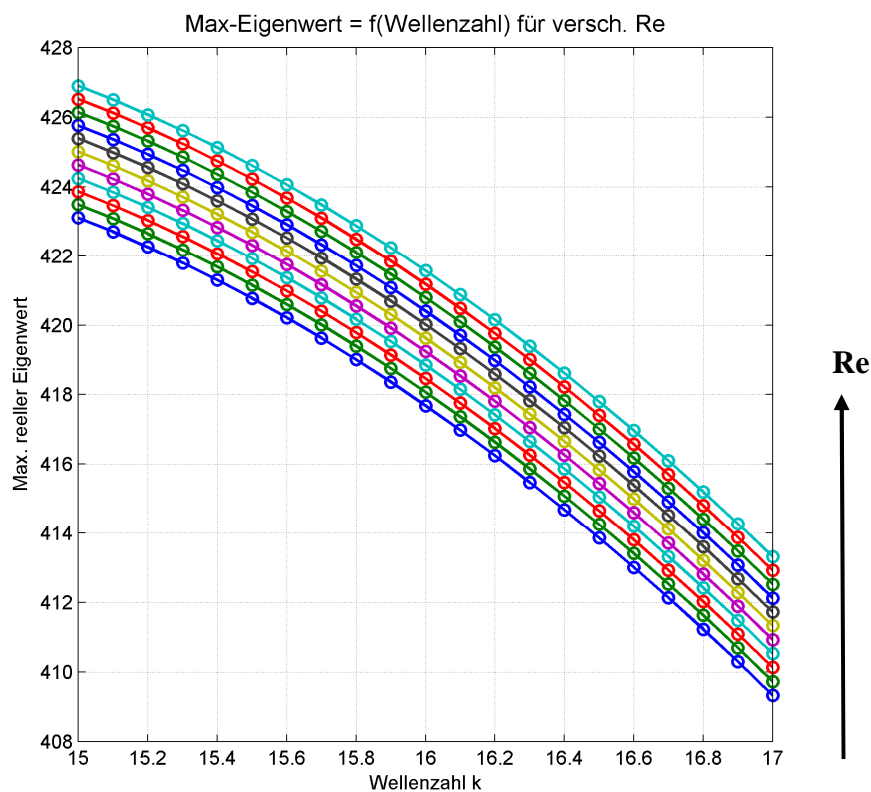

Figure 22: Truncated diagram of the maximal real eigenvalue with respect to the wave number for different Reynolds number for N = 5 equally spaced points

6.1.6 Representation of the flow field

A routine has been written which plots the vector field for a chosen maximal eigenvalue. This routine takes the eigenvector related to the chosen eigenvalue and recontructs the velocity field through building the chebyshev series, The following plots (see Figure 24) show this vector field for an overcritical flow. In this case flow the eigenvector looks as presented in Figure 23. It shows that v and ψ are out of phase as expected.

$$
\begin{bmatrix}
v_1 \\
v_2 \\
v_3 \\
v_4 \\
v_5 \\
v_6 \\
\psi_1 \\
\psi_2 \\
\psi_3 \\
\psi_4 \\
\psi_5 \\
\psi_6 \\
\psi_7 \\
\psi_8
\end{bmatrix}
\quad
\begin{aligned}
&0.9241 \\
&-0.0450 \\
&-1.0000 \\
&0.0528 \\
&0.0759 \\
&-0.0078 \\
&0 + 0.0120i \\
&0 - 0.0010i \\
&0 - 0.0160i \\
&0 + 0.0015i \\
&0 + 0.0040i \\
&0 - 0.0006i \\
&0 - 0.0000i \\
&0 + 0.0000i
\end{aligned}
$$

Figure 23: Eigenvector in an overcritical flow
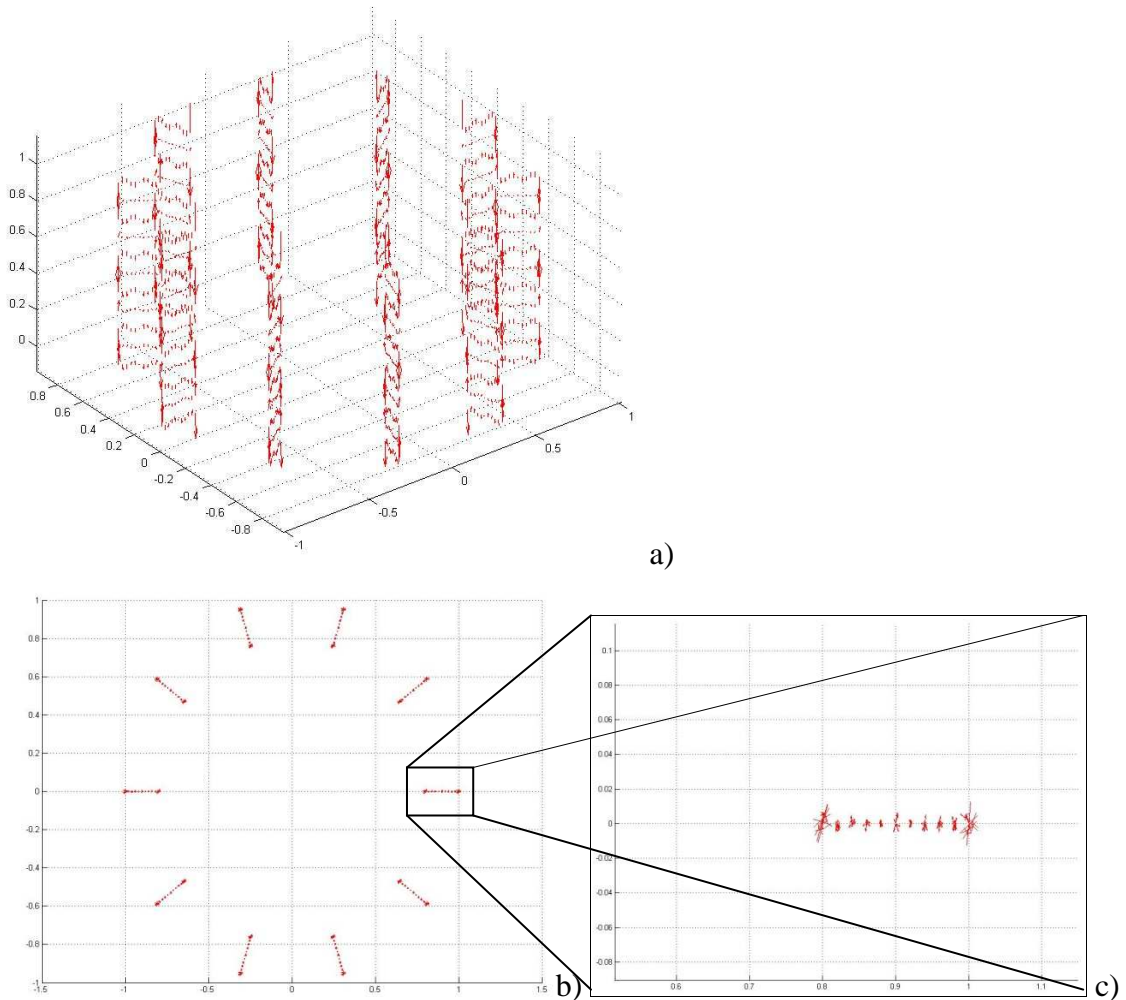

Figure 24: Vector field plot (N=5) of an overcritical eigenvector in overview a), from the top b), with zoom on the vector c)

Figure 24a) shows to a certain extend the expected vortices. Figure 24b) and c) show that the vectors captured on a plane have a component that show out of it, which is a clue for a toroidal behavior of the flow.

7   Discussion and further work

The results of carried computation of the Taylor-Couette eigenvalue problem for grades higher than 1 of Chebyshev-polynomials must be compared with literature results. As the following table shows, the computed results match really good with the literature values. It confirms the well known rapid convergence of the spectral collocation methods.

	Reynolds number (Re)	Wave number (k)
Literature values	94.7	15.65
Computed values (N = 5)	94.75	15.7

Table 10: Comparison between literature and computed values for the critical values of the Reynolds number

This analysis requires Gauss-Chebyshev or Gauß-Lobatto points instead of uniformly distributed points over the domain (results from chapter 6.1.5).

The developed routine can be adapted to any (system of) differential equation problems.

Problem can arise in the choice of the artifact-filter value λ, when approaching the critical zone. Also the choice of N should be taken carefully in order to avoid the Runge phenomenon (see Table 9)

Further work could be:

- The implementation of stop-subroutine, which would interpolate the maximal eigenvalues scanned over the wave number k and check, whether the interpolated function is tangent to the x-axe or not before the next Reynolds number is inserted in the equation.
- The implementation of a more accurate artifact-filter for near-critical-point cases.
- The implementation of a more general post processing routine, which allows the representation of any states (eigenvector) at any time.

Bibliography

[1]   Chandrasekhar, S.: Hydrodynamic and Hydromagnetic Stability. Oxford University Press (1961), New York.

[2]   Drazin, P. G.; Reid, W. H.: Hydrodynamic Stability. Cambridge University Press (1981).

[3]   Taylor, G.I.: Stability of a viscous fluid contained between two rotating cylinders. Philos. Trans. R. Soc. London, Ser. A 223, 29 (1923).

[4]   Mason, J.C; Handscomb, D.C.: Chebyshev Polynomials. Chapman & Hall/CRC (2003).

[5]   Kuhlmann, H.: Hydrodynamische Instabilität. Vorlesungsunterlagen an der TU Wien (2009). (http://www.fluid.tuwien.ac.at)

[6]   Kuhlmann, H.: Hydrodynamische Instabilität. Vorlesungsunterlagen an der Uni Bremen (1994).

[7]   Swinney, H.L.; Gollub, J.P.: Hydrodynamic Instabilities and the Transition to Turbulence. Springer Verlag (1985).

[8]   Hydrodynamic Stability Theory. Lecture note of MAGIC group in UK, spring 2007/08. (http://maths.dept.shef.ac.uk/magic/course.php?id=93)

[9]   Boyd, J.P: Chebyshev and Fourier Spectral Methods. Dover Publications, Inc, 2nd edition (2000).

[10]   Oertel, H; Delfs, J: Strömungsmechanische Instabilitäten. Springer (2005).

[11]   Taylor, M.E: Partial Differential Equations 3, Nonlinear Equations. Springer (1996).

[12]   Strogatz, S.H.: Nonlinear Dynamics and Chaos. Perseus Books Publishing, L.L.C (1994).

[13]   Trefethen, L.N: Spectral Methods in Matlab. SIAM (2000).

[14]   Baumann, B et al.: Finite Element Estimation of Acoustic Response Functions in HD Lamps. J. Phys D: Appl. Phys. 42 (2009).

[15]   Dreeben, T.D.: Modeling of Fluid-mechanical Instability in Pure-Mercury HID Lamps. Proceed. Comsol Conf. Boston (2007).

[16]   Schweizer, W.: MATLAB kompakt. Oldenbourg Verlag (2008).

[17]   Bestehorn, M.: Hydrodynamik und Strukturbildung. Springer Verlag (2006).

[18]   Rehberg, I: Phasenübergänge und Hydrodynamische Instabilitäten. Physik in unserer Zeit 12, Nr. 5, 131 (1981).

[19]   Diffo, P.: Untersuchung der linearen Stabilität der Taylor-Couette-Strömung mittels Polynomentwicklung höherer Ordnung. Master project (in English), HAW Hamburg (2011).

[20]   http://www.scholarpedia.org/article/Taylor-Couette_flow